Agronomy Research **24**(1), 27–45, 2026
https://doi.org/10.15159/AR.25.106

Estimating spring wheat nitrogen use efficiency via proximal and UAV sensing in Northwest Latvia

Z. Jansone[1,2,*], M. Bleidere[1] and G. Putniece[2]

[1]Institute of Agricultural Resources and Economics, Department of Plant breeding and Agroecology, "Dižzemes", Dižstende, LV-3258 Talsi distr., Latvia
[2]Faculty of Agriculture and Food Technology, Latvia University of Life Sciences and Technologies, 2 Liela Str., LV-3001 Jelgava, Latvia
[*]Correspondence: zaiga.jansone@arei.lv

Received: September 19th, 2025; Accepted: November 27th, 2025; Published: December 4th, 2025

Abstract. Phenotyping nitrogen use efficiency (NUE) is labour-intensive and time-consuming, often requiring destructive biomass sampling. Cost-effective sensing tools provide a promising alternative for rapid assessment of numerous wheat genotypes. In this study, sixteen spring wheat genotypes were evaluated in Latvia over three consecutive years (2021–2023) under two nitrogen fertilization levels (N75 and N150) in a split-split-plot design with two replicates, totaling 64 plots. NUE consistently differed between N rates and was strongly influenced by year-specific environmental conditions, providing contrasting scenarios for testing sensing approaches. To capture this variation, two platforms were tested for spectral estimation of NUE: a low-cost proximal phenomobile equipped with an RGB sensor, and an unmanned aerial vehicle (UAV) with a multispectral sensor. Canopy reflectance was measured at three growth stages (tillering, flowering, and milk development) to calculate 8 proximal and 9 UAV-based visible-spectrum vegetation indices (VIs). Although relationships between VIs and NUE were environmentally dependent, significant and robust correlations were found. Proximal sensing generally provided stronger prediction models, with the Normalized Green-Red Difference Index (NGRDI) and Green Area Index (GA) consistently most predictive across years. The milk development stage (GS75) proved optimal for NUE estimation. Comparisons of NGRDI between platforms demonstrated their compatibility, though UAVs offer higher throughput for large-scale phenotyping. These findings highlight the potential of integrating agronomic evaluation with canopy reflectance traits to support breeding and precision nitrogen management.

Key words: *Triticum aestivum* L., proximal and remote sensing, canopy reflectance, NUE prediction, correlation.

INTRODUCTION

Wheat (*Triticum aestivum* L.) is the most widely grown cereal globally, including in Latvia, and a major source of calories and protein. The primary goal of wheat production is to maximize grain yield while ensuring adequate protein content. Grain yield per unit area is a key indicator of productivity and nitrogen use efficiency (NUE), which optimizes nitrogen utilization and reduces environmental losses (Malinas et al.,

2022; Xu et al., 2024). NUE, defined as grain yield per unit of available nitrogen, includes nitrogen uptake efficiency (NupE), reflecting a genotype's ability to absorb nitrogen, and nitrogen utilization efficiency (NutE), which measures how effectively it uses nitrogen for grain production (Moll, et al., 1982). Evaluating NUE must consider the relationship between nitrogen and grain protein content, as efficiently remobilized nitrogen increases protein (Malinas et al., 2022). Both agronomy and breeding are crucial for improving NUE and related traits (Hawkesford & Griffiths, 2019). Since phenotyping NUE traits is labor-intensive, alternative, cost-effective methods like sensing tools are needed for rapid assessment of wheat genotypes.

In agriculture, sensor-based measurements are powerful tools for assessing crop characteristics like canopy health, growth stage, yield, biomass, nutrient status, water stress, and vegetative density (Song, et al., 2021; Gano, et al., 2024). Several studies for different crops have addressed aspects related to growing management, crop growth, and vegetation indices. For example, Domínguez et al. (2017) has demonstrated the potential of remote sensing indices to explain crop performance (e.g. yield in winter oilseed rape). Änäkkälä et al. (2023) used UAV multispectral imaging and visible-band vegetation indices to assess maize canopy traits (GLI, NDVI, etc.), demonstrating the potential of UAV-based remote sensing for phenotyping crop status under varying management. Another study, explored spatial variability in wheat using NDVI and related indices (Abreu et al., 2023).

Such non-invasive approach is essential for long-term studies and monitoring multiple plant varieties, making it especially useful for breeding programs that require rapid screening of numerous accessions (Song, et al., 2021). Sensing methods capture electromagnetic reflectance from crop canopies, influenced by plant surface properties, while spectral vegetation indices (VIs), derived from various spectral bands, quantify green vegetation. Each VI has unique advantages, limitations, and suitability for specific applications (Vidican et al., 2023).

Canopy proximal phenotyping uses sensors or imaging systems placed near the plant canopy on mobile platforms for real-time assessment of plant traits in the field (Prey et al., 2020; Rui et al., 2024). These platforms capture high-resolution data on traits like canopy height, growth, biomass, and VIs (Pour et al., 2021; Gano et al., 2024). The advancement of unmanned aerial vehicles (UAVs) has revolutionized remote sensing by capturing high-resolution images from low altitudes, providing greater flexibility than ground-based platforms (Tanaka et al., 2024). UAVs with various sensors are increasingly used to detect NUE related traits (Rasmussen et al., 2016; Quemada et al., 2019; Yang et al., 2020). VIs derived from reflectance help monitor nitrogen status and wheat performance (Prey & Schmidhalter, 2019; Fu et al., 2020), and studies show that high-resolution UAV-based RGB images can measure vegetation fractions, grain yield, physiological parameters, and nitrogen content (Fu et al., 2020; Feng et al., 2022; Prey et al., 2022; Zhang et al., 2024; Rossi et al., 2025). Building on this concept, our study evaluates visible-spectrum vegetation indices from proximal and UAV platforms to estimate nitrogen use efficiency (NUE) in spring wheat across different environments and fertilization levels.

Studies on remote phenotyping of yield and NUE related traits in wheat highlight the importance of selecting appropriate spectral indices (VIs) and optimal growth stages for measurements, as different environments have unique characteristics (Prey &

Schmidhalter, 2019; Prey et al., 2020). It is essential to evaluate the strengths and weaknesses of each VI before choosing the most suitable one for the specific environment, application, and platform. These studies show that there is an established interest in nitrogen effects on cereal crops, remote sensing and/or indices, but to our knowledge none have directly compared proximal vs UAV-based visible-spectrum vegetation indices across multiple growth stages for prediction of NUE in spring wheat over multiple years, which is what we aim to do in current study.

The first results on UAV multispectral estimation of grain yield (GY) under different N rates in Nordic–Baltic environments are available at Jansone et al. (2024). Our paper focuses on nitrogen use efficiency (NUE) estimated at maturity for the same set of spring wheat genotypes grown under two nitrogen fertilization levels over three years in Latvia.

The objectives were to (1) evaluate nitrogen use efficiency (NUE) under contrasting nitrogen fertilization rates (N75 and N150) across multiple environments; (2) identify the most suitable visible-spectrum vegetation indices (VIs) and optimal growth stages for predicting NUE in spring wheat, (3) explore correlations between NUE traits and selected VIs across environments to assess their robustness, and (4) compare the predictive performance of proximal (RGB phenomobile) and UAV-based (multispectral) sensing platforms for estimating NUE. This research offers valuable insights into using spectral indices for breeding and precision phenotyping.

MATERIALS AND METHODS

Experimental site and methods

Field trials were conducted at the AREI Stende Research Centre experimental site in northwest Latvia (57°18′ N, 22°56′ E; WGS84 coordinate system) during the 2021–2023 growing seasons (Fig.1, b). Trials were established as a split-split-plot design including 16 spring wheat genotypes arranged in two randomized replicates (R1 and R2) with two nitrogen fertilization levels (N75 and N150), for a total of 64 plots (Fig. 1, a; Table 1).

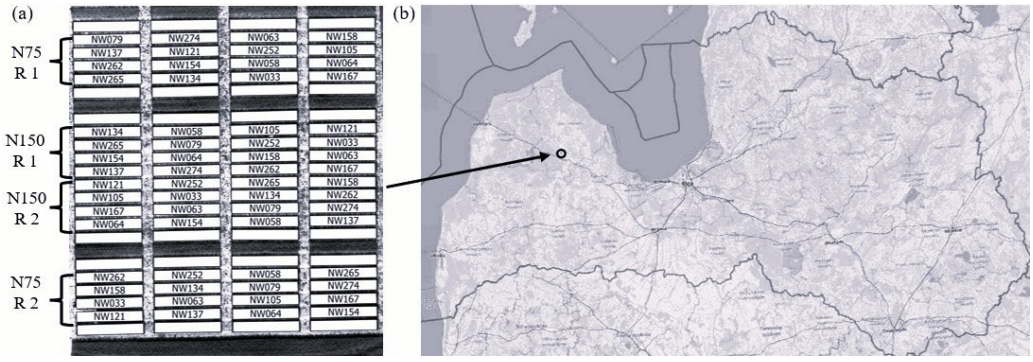

Figure 1. (a) The experiment design of established trials; (b) geographical location of study area.

The main plots represented nitrogen (N) rates, while sub-plots were assigned to wheat genotypes. A detailed description of the 16 varieties and breeding lines from Latvia, Lithuania, Estonia, and Norway is provided in the previous study (Jansone et al., 2024). Two N fertilization rates (75 kg ha^{-1} N for N75 and 150 kg ha^{-1} N for N150) were applied before sowing. The field consisted primarily of homogeneous Albeluvisol (eutric) sandy loam. Spring wheat was sown at a density of 500 germinable seeds per m^2 in rows spaced 12.5 cm apart. Plots were 1.2 m wide and 8.4 m long. Trials were conducted between 23 April and 2 May each year, depending on weather conditions. Pesticides, including herbicides, foliar fungicides, and insecticides (if needed), were applied.

Table 1. Spring wheat varieties and breeding lines used in the study

Genotype name	Provider*	Country of origin
Runar	NMBU	Norway
Zombi	Graminor	Norway
Caress	NMBU	Sweden
Betong	Graminor	Norway
Hiie	METK	Estonia
Voore	METK	Estonia
876	METK	Estonia
990-2	METK	Estonia
Robijs	AREI	Latvia
013-032	AREI	Latvia
013-01	AREI	Latvia
013-074	AREI	Latvia
DS-17-16-DH	LAMMC	Lithuania
DS-638-5-DH	LAMMC	Lithuania
DS-655-7-DH	LAMMC	Lithuania
DS-720-3-DH	LAMMC	Lithuania

*NMBU – Norwegian University of Life Sciences; METK – Centre of Estonian Rural Research and Knowledge; AREI – Agricultural resources and Economics; LAMMC – Research Centre for Agriculture and Forestry.

Meteorological conditions varied each year: precipitation from May to August was 334 mm in 2021, 332 mm in 2022, and 238 mm in 2023, compared to the 30-year long-term average (LTA) of 274 mm. 2021 had lower temperatures in April, May, and August, but higher temperatures in June and July (4.2 °C and 4.6 °C above LTA). In 2022, temperatures were cooler in April and May, with June exceeding the LTA by 2.0 °C, and precipitation in June was 68% of the LTA. In 2023, May was cool and rainfall in May and June was low (11% and 6% of the LTA), affecting nutrient uptake and causing nitrogen deficiency, but July temperatures were slightly below the LTA with sufficient moisture.

Acquisition of ground data:

Plant measurements and calculation of N use efficiency trait

Development stages for each genotype were recorded to provide an accurate timing for destructive plant sampling. Above-ground plant samples were collected from a 0.1 m² area in the center of each 8×1.2 m plot at physiological maturity, prior to mechanical harvest, to determine total biomass and nitrogen concentration for NUE calculation. Plant samples were weighed, grains were threshed and weighted, and samples of both grain and straw biomass were analysed for the total N concentration using the Kjeldahl method (ISO 20483:2013) expressed on an oven–dried weight basis. The dry matter content of grain and straw biomass samples was determined after oven drying at 130 °C for 2 hours (ISO 712:2009).

Nitrogen use efficiency (NUE) was computed as the grain yield per unit of the N supply, which comprises both uptake efficiency (*NUpE*) and utilization efficiency (*NUtE*) (Moll et al., 1982) (1):

$$NUE = NUpE \times NUtE = \frac{Nt}{Ns} \times \frac{GDM}{Nt} \quad (1)$$

where, *GDM* is grain dry mass per unit area, *Nt* is total above-ground plant biomass N, including grain N concentration (NG) and straw biomass N concentration (NB) at maturity per unit area, and *Ns* is N supply including the available N in the soil and applied N from fertilizer per unit area. *GDM*, *Nt*, and *Ns* are all expressed in the same units. NG and NB were determined by the Kjeldahl-N analysis and was expressed on a dry weight basis. The available nitrogen (N) in the soil was considered to be the total mineral N concentration in the upper 0.2 m of the soil profile, as determined before sowing and calculated taking into account the soil bulk density. The total N concentration in the soil samples were determined by the Modified Kjeldahl method (ISO 11261:2002).

Spectral data acquisition and processing

Proximal (phenomobile) and UAV-based spectral measurements were performed three times during each trial year, corresponding to specific stages of plant vegetative and generative development based on the Zadoks growth scale – tillering (growth stage 25/GS25), flowering (GS65), and milk development stage (GS75) (Table 2). The developmental stages varied slightly between genotypes due to differences in phenological development.

Table 2. Dates of spectral measurements during dominant growth stages

Phenotyping platforms	Growth stage	2021	2022	2023
Phenomobile	Tillering (GS25)	05/31	05/26	05/25
	Flowering (GS65)	06/28	07/01	06/27
	Milk development (GS75)	07/15	07/19	07/13
Unmanned aerial vehicle	Tillering (GS25)	05/29	05/25	05/23
	Flowering (GS65)	06/29	06/30	06/26
	Milk development (GS75)	07/13	07/18	07/11

Although the proximal (phenomobile) and UAV measurements were not always performed on the same calendar day due to slight differences in phenological development among genotypes, all measurements were conducted under similar environmental conditions (clear skies, low wind) and corresponded to the same dominant growth stage. This approach minimized short-term environmental variability and ensured reliable comparison of vegetation indices across platforms.

A low-cost sensing plant phenotyping platform (phenomobile) was used for spring wheat canopy proximal phenotyping, equipped with a consumer-grade RGB camera, the Canon EOS 1300D, and a focal length of 18 mm (Fig. 2, a).

Images were saved in high-resolution (4,288×2,848 pixel) JPEG format. One picture per plot (from the middle part of the plot) was captured. A white balance card (WBC), placed at same height as the canopy, was positioned in the corner of each image taken by the camera by using a cardholder on phenomobile. The height between the ground and the camera was fixed at 2 meters, consistent across all growth stages and years. After the white balance corrections, the WBC was cropped out of the images.

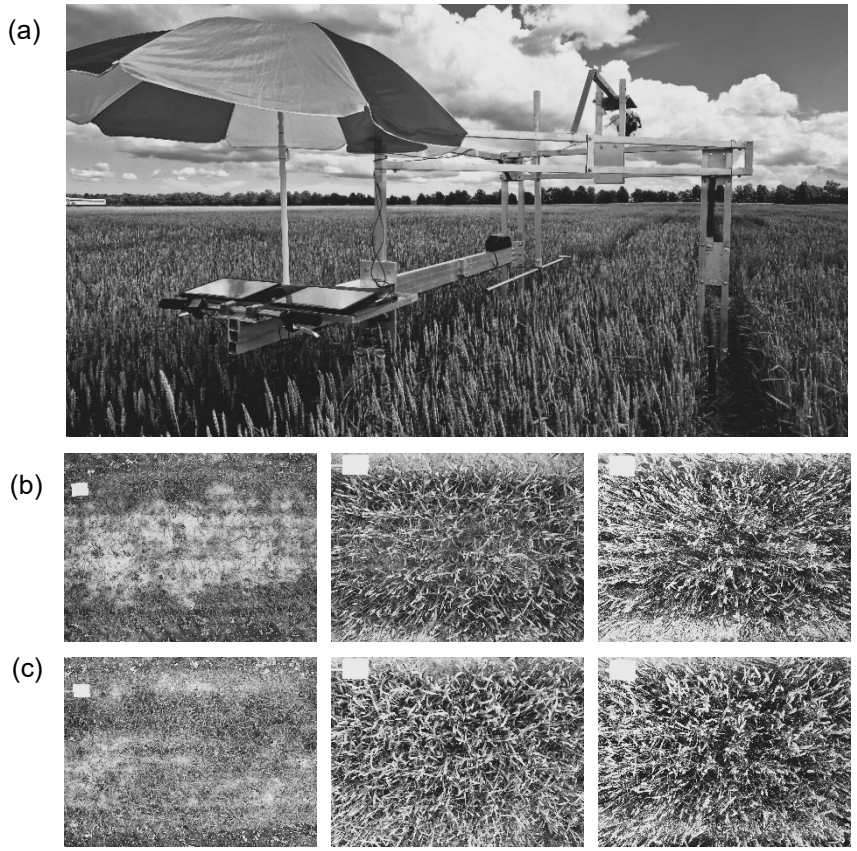

Figure 2. Proximal image acquisition using a low-cost phenomobile for spring wheat canopy phenotyping. (a) Phenomobile platform used for proximal sensing at the flowering stage (GS65); (b) Representative canopy images with a white balance card captured at tillering (GS25), flowering (GS65), and milk development (GS75) growth stages under the N75 fertilization level; (c) Representative canopy images with a white balance card captured at GS25, GS65, and GS75 under the N150 fertilization level.

The CerealScanner plugin (University of Barcelona), utilizing ImageJ software, was used to analyze images and generate RGB vegetation indices from the proximal phenotyping platform (Kefauver, 2018; Kefauver et al., 2020). It incorporates the hue, saturation, and intensity (HSI) model to quantify plant properties. Indices such as Green Area (GA) and Greener Green Area (GGA) were calculated by classifying pixels as green, with GA including yellow to bluish-green tones, and GGA focusing on a narrower range excluding yellowish-green. The Crop Senescence Index (CSI) combines these indices to assess senescence (Kefauver et al., 2020). Two additional vegetation index adaptations, NGRDIveg and TGIveg, were derived from the original NGRDI and TGI formulas, respectively (Table 3). These indices were calculated by applying a vegetation mask (NGRDI > 0) to include only vegetation pixels, thereby minimizing soil background effects and improving the accuracy of canopy reflectance estimates (Hamdane et al., 2023).

Table 3. Vegetation indices (VIs) derived from RGB images captured by the phenomobile

Abbr.	Vegetation indices	Formula	Reference
HUE	The main component of the hue, saturation, and intensity (HSI) color model that represents the actual color of an object	The color value, measured as an angle between 0° and 360° on the visible spectrum	Kefauver et al., 2020
GA	Green Area Index	60 < HUE < 180	Jauregui-Besó et al., 2025
GGA	Greener Green Area Index	80 < HUE < 180	Jauregui-Besó et al., 2025
CSI	Crop Senescence Index	100(GA-GGA)/GA	Hamdane et al., 2023
NGRDI	Normalized Green-Red Difference Index	(G-R)/(G+R)	Jauregui-Besó et al., 2025
TGI	Triangular Greenness Index	-0.5(190(R-G)-120(G-B))	Jauregui-Besó et al., 2025

R – red, G – green, B – blue. Red, Green, and Blue are the digital number values in the respective channels extracted from the orthophotos.

A commercial UAV model, the DJI Phantom 4 Multispectral quadcopter (DJI, Inc.,Shenzhen, Guangdong, China), was used to capture images from an altitude of 20 m and with a ground sample distance (GSD) of 1 cm (Fig. 3, a). The images were taken with a minimum of 75% overlap in both the front and side directions, using a 90-degree (NADIR) camera position. Each flight mission generated approximately 5,000 TIFF images, with five images captured for each shot. The result was a series of average reflectance values for field trial plots across five spectral bands: red, green, blue, red edge, and near-infrared. Aerial images were processed using PIX4Dmapper by Pix4D (Switzerland), with orthophotos georeferenced to an RMSE of 3–5 cm. Ground control points (GCPs) were established and maintained throughout the vegetation season to ensure precision (Fig. 3, b). For each flight, a multispectral photo of the MAPIR calibration panel was captured to standardize results across locations and missions. Spectral reflectance values were

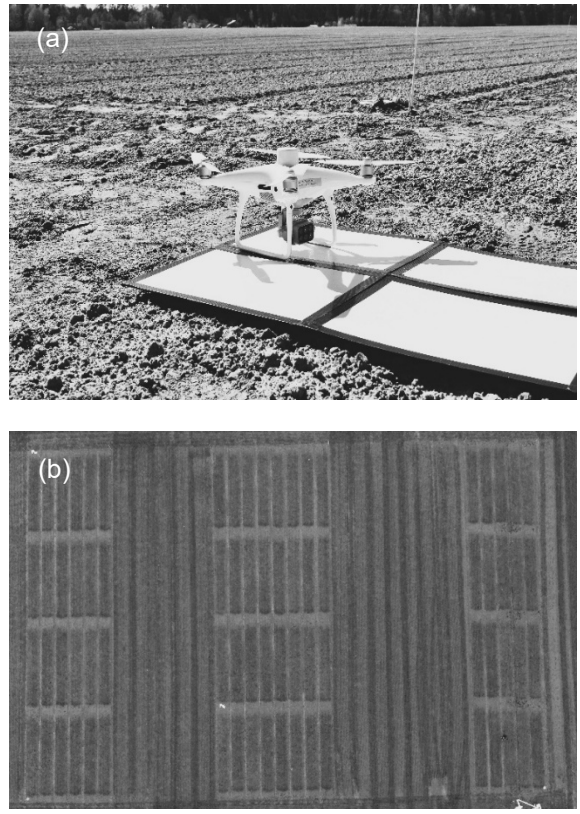

Figure 3. UAV-based remote sensing platform and orthophoto of the spring wheat field trial. (a) UAV-based multispectral platform before flight mission. (b) UAV-derived orthophoto of the field trial at the tillering stage (GS25), showing ground control points and the split-split-plot design with 16 spring wheat genotypes arranged in two replicates and two nitrogen fertilization levels (N75 on both sides and N150 in the middle), totalling 64 plots.

extracted from the orthophoto mosaics, cropped to field boundaries, and analysed using. QGIS zonal statistics. A vector layer was created using a georeferenced orthophoto image to delineate trial plots

A total of nine visible band vegetation indices, captured from UAV images, were calculated based on a literature review of related previous studies (Table 4).

Table 4. Vegetation indices (VIs) derived from red green blue (RGB) images by unmanned aerial vehicle

Abbr.	Vegetation indices	Formula	Reference
NGRDI	Normalized Green-Red Difference Index	(G-R)/(G+R)	Rasmussen et al., 2016
GRRI	Green-Red Ratio Index	G/R	Du & Noguchi, 2017
NGBDI	Normalized Green-Blue Difference Index	(G-B)/(G+B)	Rossi et al., 2025
ExG	Excess Green Index	2G-R-B	Li et al., 2022
VDVI	Visible-Band Difference Vegetation Index	(2G-R-B)/(2G+R+B)	Wang et al., 2013
BGI	Blue Green Pigment Index	B/G	Prey & Schmidhalter, 2019
BRI	Blue-Red Pigment Index	B/R	Prey & Schmidhalter, 2019
GMR	Green Minus Red Index	G-R	Wang et al., 2013
VARI	Visible Atmospherically Resistance Index	(G-R)/(G+R-B)	Rossi et al., 2025

R – red, G – green, B – blue. Red, Green, and Blue are the digital number values in the respective channels extracted from the orthophotos.

Statistical analysis

Although genetic variation in nitrogen use efficiency (NUE) was observed among the 16 spring barley genotypes, the selection of vegetation indices (VIs) and growth stages was based on the combined dataset across all genotypes to identify indices robust for general NUE prediction.

The simple linear regression was used to develop predictive models for NUE based on individual VIs (2):

$$y = a + bx \tag{2}$$

where, *y* is the predicted trait (e.g., NUE), x is the predictor (VI), b is the slope, and a is the intercept.

Model performance was evaluated using Pearson correlation coefficient (*r*), the coefficient of determination (R^2), and root mean square error (RMSE).

Pearson correlation coefficient (r) quantified the strength and direction of linear relationships between variables (3):

$$r = \frac{\sum(x_i - x)\,(y_i - y)}{\sqrt{\sum(x_i - x)^2 \sum\left((y_i - y)\right)^2}} \tag{3}$$

where x_i and y_i represent the observed values of variables x and y for observation *i*, while x and $\bar{y}$ denote the mean values of the respective variables, the resulting Pearson correlation coefficient r ranges from −1 to 1, with values close to 1 indicating a strong positive linear relationship, values near −1 indicating a strong negative relationship, and values around 0 suggesting no linear association.

The model accuracy was assessed using the coefficient of determination (R^2), root mean square error (RMSE). The coefficient R^2 gauges the alignment between the estimated and measured values. R^2 represents the proportion of variance in the dependent variable explained by the model and ranges from 0 to 1, a value closer to 1 signifies a better model fit.

The coefficient of determination (R^2) was calculated as (4):

$$R^2 = 1 - \frac{\sum(y_i - \hat{y}_i)^2}{\sum(y_i - y_i)^2} \quad (4)$$

Root mean square error (RMSE) measured the average prediction error to quantify model accuracy (5):

$$\text{RMSE} = \sqrt{\frac{\sum(y_i - \hat{y}_i)^2}{n}} \quad (5)$$

where y_i denotes the observed value for observation $\hat{y}_i$ represents the model-predicted value for the same observation, and n is the total number of observations. RMSE quantifies the average difference between predicted and observed values. Lower values of RMSE indicate better model fit. Its units are the same as the dependent variable (e.g., kg ha^{-1} for NUE).

The best regression models for NUE prediction were defined as those exhibiting the highest R^2 and lowest RMSE values.

For each growth stage, RMSE values were used to rank the VIs for their predictive ability of NUE (Eq. 6). Ranking of vegetation indices (VI) (6):

$$Rank_{norm} = \frac{Rank - Rank_{min}}{Rank_{max} - Rank_{min}} \quad (6)$$

The best-performing VI received the lowest rank. To account for differences across growth stages, ranks were normalized for each stage and summed to produce a total rank sum for each VI (7):

$$Total\ Rank\ Sum = \sum_{stages} Rank_{norm} \quad (7)$$

Higher total rank sums indicate better overall predictive performance across stages.

All analyses were conducted using the Real Statistics add-in for MS Excel and R statistical software version 4.2.3 (R Core Team, 2021), utilizing the packages: *lmridge, tidyverse, corrr, ggplot2*, and *ggpubr*.

RESULTS AND DISCUSSION

Implementing affordable high-throughput phenotyping tools to monitor wheat traits throughout growth stages provides valuable insights for breeders investigating genotype-phenotype correlations. This study offers an opportunity to validate VIs under contracting management and environmental conditions. This paper identifies an optimal set of RGB VIs for nitrogen use efficiency in spring wheat, evaluating their performance under low and high N fertilization conditions. Because sensor data can be influenced by lighting, platform inconsistencies, and canopy structural changes at different growth stages, identifying robust indices is essential.

Nitrogen use efficiency under contrasting nitrogen rates and environments

Nitrogen use efficiency (NUE) showed pronounced variation between nitrogen fertilization levels, years, and genotypes (Fig. 4). Across all six environments (three years × two N levels), NUE was consistently higher at the reduced fertilization rate (N75) compared to the higher input (N150). In 2021, mean NUE reached 30.6 kg grain kg N^{-1} under N75, while it decreased to 20.1 kg grain kg N^{-1} under N150. In 2022, the highest values were recorded, with 50.2 and 28.9 kg grain kg N^{-1} at N75 and N150, respectively. In 2023, NUE was again higher under N75 (32.2) than N150 (19.5). The differences between nitrogen treatments were statistically significant ($P < 0.05$) within each year. Boxplots further revealed considerable phenotypic variation among the 16 genotypes, indicating genetic diversity in the capacity to utilize nitrogen efficiently.

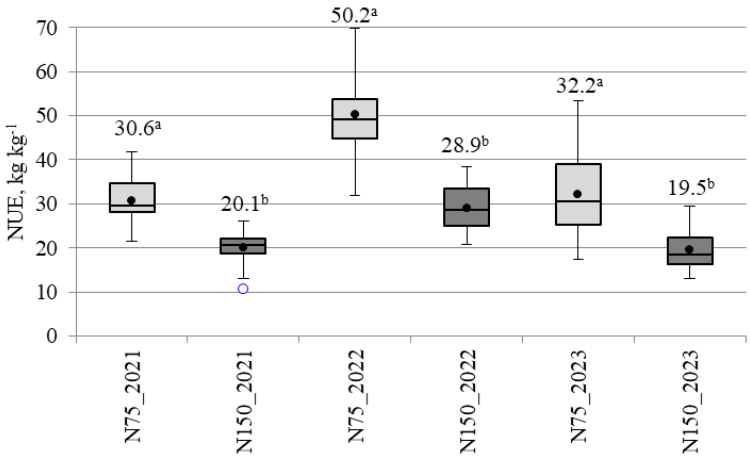

Figure 4. Boxplot showing the phenotypic distribution of Nitrogen use efficiency (NUE) for 16 spring wheat genotypes grown in six environments. The black horizontal line in each boxplot is the median, the lower and upper box edges are the first and third quartiles, respectively, and the whiskers are the data minimum and maximum. The black circle in each plot is the mean for that class. Outliers are shown as open circles; 2021, 2022 and 2023–year of trials; N75–N rate with 75 kg N ha^{-1}; N150–N rate with 150 kg N ha^{-1}; a, b–significant differences ($P < 0.05$) between the mean values of two N rates within each year are shown by different superscript letters.

The strong year-to-year variation was closely related to meteorological conditions. In 2021, although precipitation (334 mm) was above the 30-year long-term average (274 mm), elevated temperatures in June and July (+4.2 °C and +4.6 °C above LTA, respectively) likely accelerated crop development, limiting the time for N uptake and reducing NUE under higher fertilization. In 2022, rainfall was near average (332 mm) and temperatures during grain filling were favorable, which likely contributed to the highest NUE values observed across the study. In contrast, 2023 was characterized by exceptionally dry conditions in May and June (11% and 6% of LTA precipitation), which restricted nutrient uptake and caused visible nitrogen deficiency symptoms, resulting in markedly lower NUE despite adequate rainfall in July. These results confirm the strong environmental dependence of NUE and are consistent with earlier findings that nitrogen efficiency in cereals is highly sensitive to seasonal weather patterns and soil moisture availability (Frels et al., 2018; De Santis et al., 2025).

The decline in NUE under higher nitrogen rates (N150) across all years highlights the diminishing returns of excessive N fertilization. Results of Litke et al (2018) obtained also in Latvian conditions indicated that the nitrogen fertilizer rate affected significantly ($P < 0.001$) NUE, and higher NUE was in the variants with the lowest nitrogen rates. It demonstrating that increased N input beyond crop demand can lower N efficiency in cereals, primarily due to limited uptake and higher losses. From an agronomic perspective, these findings underscore the importance of identifying wheat genotypes capable of maintaining high NUE under reduced nitrogen supply.

Identifying optimal visible light spectral VIs and growth stages for predicting NUE

The observed phenotypic variation in nitrogen use efficiency (NUE), with consistently higher values under N75 and strong year-to-year dependence on meteorological conditions, provides a solid basis for evaluating the capacity of VIs to capture these agronomic differences. Such an approach aligns with previous work showing that optical/photometric diagnostics can effectively reflect crop nitrogen status under varied fertilization in spring barley and rapeseed (Shchuklina et al., 2022). Also, the study on evaluation of useability of vegetation indices has employed UAV plus RGB multispectral imaging and proximal sensors to monitor crop leaf properties and canopy structure in different phenological stages (Jelínek et al., 2020). The research on wheat demonstrated that various image features derived from UAV RGB images, including RGB-based vegetation indices (VIs) and color parameters, can effectively estimate the nitrogen status (Fu et al., 2020). Timing is crucial for obtaining accurate phenotyping results (Prey et al., 2020). Together, these studies help frame our analysis of how proximal and UAV-based spectral tools can estimate NUE reliably across environments.

We are particularly focused on vegetation indices (VIs) strongly linked to nitrogen use efficiency (NUE) that remain consistent across different environments. The three highest-ranking VIs for the NUE trait, based on the summed rank across growth stages in 2021, 2022, and 2023 are presented in Table 5.

The top ranked VIs varied depending on growth stage and environmental factors (N fertilizer rate and year of investigation). In 2021 RMSE was lowest for VI prediction of NUE at flowering (GS65) and at the milk development stage (GS73), under high N (N150) conditions. In 2022 RMSE was lowest for VI prediction of NUE trait under both low and high N treatments. In turn in 2023 RMSE was lowest for VI prediction of NUE trait at GS65 and GS75, but only under N75 fertilization rate. The highest ranked VI for NUE trait was different for each environment. Common VIs often was identified among the three most predictive indices base on ranking results in the varied environments.

The Normalized Green-Red Difference Index (NGRDI) was the vegetative index consistently identified as the most predictive over the three-year study period. In 2021, at GS75, NGRDI accounted for 23% of the NUE variation, while it explained 29% in 2022 and 55% in 2023. The NGRDI index, proposed by Hunt et al., 2005 to assess dry biomass and nutrient status, is similar to the NDVI but uses the green and red bands instead of the red and near-infrared (NIR) bands.

Table 5. Root mean square error (RMSE), and rank (R) for VI and NUE regression in three years of investigation

VI	Growing stage									SR
	GS25			GS65			GS75			
	RMSE	R^2	*R*	RMSE	R^2	*R*	RMSE	R^2	*R*	
2021										
N75										
HUE	0.24	0.04ns	3	0.24	0.05ns	7	0.24	0.02ns	6	16
GA	0.24	0.03ns	4	0.23	0.11ns	3	0.24	0.02ns	2	9
GGA	0.24	0.01ns	7	0.22	0.20**	1	0.24	0.01ns	10	18
N150										
NGRDI[2]	0.21	0.09ns	6	0.19	0.22**	3	0.19	0.23**	3	12
GRRI	0.21	0.10 *	4	0.19	0.21**	4	0.19	0.22**	6	14
VARI	0.21	0.09	5	0.19	0.20**	5	0.19	0.22**	5	15
2022										
N75										
HUE	0.20	0.09ns	6	0.20	0.06ns	3	0.18	0.28**	4	13
GA	0.19	0.14*	1	0.21	0.02ns	10	0.17	0.31***	1	12
NGRDI[1]	0.20	0.10ns	4	0.21	0.02ns	11	0.18	0.29**	3	18
N150										
NGBDI	0.27	0.05ns	5	0.28	0.02ns	7	0.26	0.17*	3	15
ExG	0.27	0.05ns	4	0.28	0.05ns	2	0.25	0.23**	1	7
BGI	0.27	0.05ns	6	0.28	0.02ns	8	0.26	0.17*	2	16
2023										
N75										
VDVI	0.25	0.06ns	7	0.22	0.30*	5	0.19	0.46**	5	17
GA	0.25	0.04ns	12	0.21	0.31*	4	0.16	0.60***	2	18
NGRDI[1]	0.26	0.01ns	14	0.20	0.37*	1	0.17	0.55**	4	19
N150										
HUE	0.25	0.05ns	3	0.24	0.10ns	3	0.25	0.03ns	12	18
GGA	0.25	0.02ns	6	0.24	0.11ns	2	0.25	0.05ns	10	18
NGRDI[1]	0.25	0.04ns	4	0.25	0.08ns	4	0.25	0.06ns	9	17

3 years – 2021, 2022 and 2023; 2 N levels – N75: 75 kg N ha^{-1}, N150: 150 kg N ha^{-1}; across four crop growth stages (GS): GS25 – tillering growth stage; GS65 – flowering growth stage; GS75 – milk development growth stage; R^2 - determination coefficients, SR – Summed Rank; HUE – the main component of the hue, saturation, and intensity (HSI) color model that represents the actual color of an object; GA – Green Area Index; GGA – Greener Green Area Index; NGRDI – Normalized Green-Red Difference Index; GRRI – Green–Red Ratio Index; VARI – Visible Atmospherically Resistant Index; NGBDI – Normalized Green-Blue Difference Index; ExG – Excess Green Index; BGI – Blue Green Pigment Index; VDVI – Visible-Band Difference Vegetation Index; [1]Phenomobile; [2] UAV, ***P<0.001; **P<0.01; *P<0.05; ns – non-significant.

This approach enables the use of lightweight digital cameras due to spectral differences between vegetation and soil, though it has certain limitations. A study on wheat found that UAV-based remotely sensed multispectral traits were more effective in predicting variations in NUE among genotypes (Yang et al., 2020). Although NGRDI, recorded using UAV as a reliable replacement for destructive measurements, showed high r values, they concluded that multispectral indices containing the near-infrared band, such as NDVI, GNDVI, NDRE, and RECI, were more sensitive for NUE prediction. Similarly, a study by Kefauver et al., 2017 indicated that different multispectral indices

are often more complementary in a multivariate model than the quantification provided by high-resolution RGB, which covers only broad electromagnetic regions within the visible spectrum. In the study by Prey & Schmidhalter, 2019, a quantitative index ranking was used to assess growth stage-independent indices. They found that near-infrared (NIR) and red-edge indices were particularly effective for estimating grain and total nitrogen uptake, outperforming traditional visible light indices.

The study also noted that the ear emergence and anthesis phases were less effective for detecting grain N uptake due to variations in plant development. Similar to our findings, it was concluded that the milk development stage is optimal for spectral measurements, offering the best relationships for estimating N use traits, while stem elongation also showed promise for earlier estimations (Prey et al., 2020). Biomass dry matter is closely linked to NUE, as higher biomass per unit of nitrogen indicates higher NUE, making biomass a key indicator for assessing nitrogen efficiency. A remote sensing study with NGRDI found that dry biomass in crops like soybeans and corn was linearly correlated with this visible light index up to a certain biomass threshold, beyond which NGRDI saturated, indicating it could no longer capture additional biomass variation. Additionally, in a corn fertilization experiment, NGRDI did not reflect nitrogen status differences despite visible low nitrogen areas in late-season images (Hunt et al., 2005).

Green Area Index (GA) was another one VIs identified as the most predictive over the three-year study period. GA at GS75 explained 2%, 31%, and 60% of the NUE variation over the three years of the study, respectively (Table 4). Casadesu et al., 2007 found a high correlation between RGB VIs (e.g., GA, GGA) and NDVI. In rainfed conditions, each visible light VI provided estimations similar to or slightly better than NDVI. However, in high-productivity conditions during anthesis, neither the RGB VIs nor NDVI accurately estimated productivity, likely due to VI saturation in areas with full soil cover and high plant density.

The Visible Atmospherically Resistant Index (VARI) is commonly used for vegetation data collection with RGB cameras. In our study, we did not select VARI as index a consistently correlated with NUE, as it provided significant regression only in 2021, at both the flowering and milk development stages (Table 4). However, other studies have shown strong correlations with VARI at the tillering stage (Ge et al., 2021) and the initial grain-filling stage (Liu et al., 2022).

In general, in our study the vegetation indices obtained from the proximal platform provided a comparatively better NUE prediction model. It should be noted that in 2021 and 2022, at the high fertilization rate, only the vegetation indices obtained from UAVs were at the top of the RMSE ranking. Prey & Schmidhalter, 2019 highlighted that while spectral proximal sensing can optimize nitrogen management in wheat cultivation, improvements in index selection and understanding of plant traits are needed. This is because nitrogen partitioning to the grain is not always detectable by sensors, limiting the effectiveness of spectral sensing methods.

Correlation between NUE trait and selected VIs across varied environments

Correlation analysis was conducted to evaluate the relationships between NUE and the four most predictive VIs under contrasting N rates and over three years environmental conditions: ExG and VDVI obtained from the UAV sensing platform, and GA and NGRDI from the phenomobile (Table 6).

Table 6. Correlation between NUE and selected VI across nitrogen rates and years

Year	N rate	GS	ExG	VDVI	GA	NGRDI Ph
2021	N75	GS25	0.028	-0.072	-0.178	-0.032
		GS65	-0.270	-0.007	0.328	0.276
		GS75	0.055	0.111	0.148	0.123
	N150	GS25	-0.364*	-0.316	-0.325	-0.268
		GS65	-0.130	0.303	0.517**	0.480**
		GS75	0.349	0.418*	0.472**	0.463**
2022	N75	GS25	0.295	0.277	0.376*	0.320
		GS65	0.070	-0.159	0.155	-0.132
		GS75	0.191	0.198	0.557***	0.539**
	N150	GS25	-0.230	-0.186	-0.132	-0.032
		GS65	-0.220	-0.039	0.035	-0.035
		GS75	-0.479**	0.035	0.322	0.355*
2023	N75	GS25	-0.438*	-0.413*	-0.364*	-0.384*
		GS65	-0.225	0.604***	0.609***	0.612***
		GS75	0.288	0.662***	0.638***	0.717***
	N150	GS25	-0.281	-0.246	-0.193	-0.118
		GS65	0.091	0.546*	0.560*	0.610*
		GS75	0.367	0.681**	0.776***	0.741***

3 years – 2021, 2022 and 2023; 2 N levels – N75: 75 kg N ha^{-1}, N150: 150 kg N ha^{-1}; across four crop growth stages (GS): GS25 – tillering growth stage; GS65 – flowering growth stage; GS75 – milk development growth stage; ExG – Excess Green Index; VDVI – Visible-Band Difference Vegetation Index; GA – Green Area Index; NGRDI Ph – Normalized Green-Red Difference Index calculated from Phenomobile images; ***P<0.001; **P<0.01; *P<0.05; ns – non-significant.

In all years of the study, VIs such as VDVI, GA, and NGRDI were most strongly correlated with NUE at Zadoks growth stage 75 (GS75). However, unlike in 2021 and 2022, in the 2023 environment, these same VIs were also correlated with NUE at the flowering stage (GS65) under both N rates. In another study of wheat N use traits under four nitrogen treatments across two experimental sites, the Normalized Green-Red Difference Index (NGRDI) showed low correlations with N-content at flowering and maturity in high N treatments (180–240 kg N ha^{-1}), but strong correlations (r = 0.81 to 0.89) in low N treatments (0–120 kg N ha^{-1}) (Yang et al., 2020). Vegetation indices in spring wheat strongly correlated with NUE at the jointing stage (GS30 on the Zadoks scale, when the first signs of stem elongation are visible) from visible light indices with also NGRDI showing the highest correlation coefficient (Liu et al., 2022). All selected VIs, except ExG, were mostly positively correlated with NUE at GS65 and GS75. Overall, the ExG index demonstrated variability in the correlation relationship across different environments.

In all years of the study, at the early stage of development (GS25), the rank-based best VIs showed mostly negative correlation relationships with the NUE trait. The Pearson correlation analysis was performed between RGB-VIs from UAV images and plant N concentration also across rice growth stages. At the jointing stage, very strong correlations were observed with Green-Red Ratio Index (GRRI) (r = 0.89) and NGRDI (r = 0.89). At the flowering stage, GRRI showed the highest correlation with N content (r = 0.84) among all RGB-VIs (Ge et al., 2021). The study of Prey at al., 2020 noted

that index differentiation was most pronounced in the highest-yielding year, highlighting the impact of environmental conditions on spectral data and the importance of year-specific calibration.

Comparison of Visible Spectrum VIs Performance: Proximal vs. UAV-Based Remote Sensing Platforms

According to the results of regression analysis (Table 4), the VIs obtained with the proximal platform (phenomobile) were most frequently found at the top three of the ranking. To compare the results between the two phenotyping platforms, we used NGRDI, calculating the correlation between the VIs obtained from the unmanned aerial vehicle (NGRDI_UAV) and the phenomobile (NGRDI_Ph) by each year of investigation (Fig. 5).

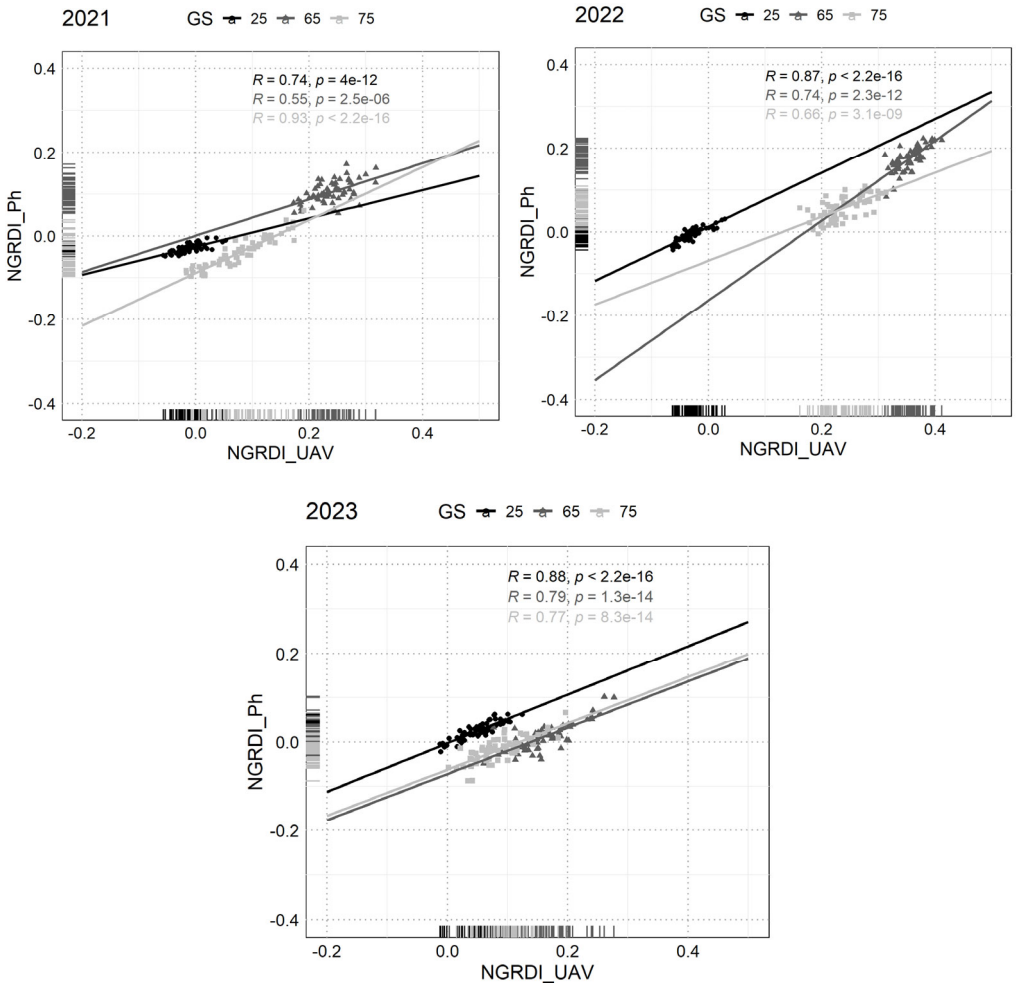

Figure 5. Relationship between Normalized Green-Red Difference Index obtained from the unmanned aerial vehicle (NGRDI_UAV) and the phenomobile (NGRDI_Ph) in 2021, 2022 and 2023.

High regression coefficients (R^2 = 0.56–0.93) were obtained withing all years of the study, indicating the comparability of the sensor results from both platforms. Minor discrepancies in the data alignment between the two platforms may arise because measurements in certain years and plant development stages differed by one to two days (Table 1). A study on barley also compared UAV-based and field-based high-throughput plant phenotyping using the free, open-source image analysis software FIJI. This analysis utilized RGB images from conventional digital cameras in combination with a matching set of ground sensors. The highest correlations with final grain yield came from the GGA and GA indices from RGB images taken at the ground level followed closely by the same indices measured from the UAV aerial platform (Kefauver et al., 2017). Two sensing systems including RGB and a multispectral camera were compared in the study of Quemada et al., 2019. The findings indicate that the use of optical sensors, both at ground level and from unmanned aerial vehicles (UAVs), can significantly enhance the understanding of crop nitrogen status and yield potential. They concluded that VIs obtained from ground measurements were highly correlated with those from the aerial platform.

CONCLUSIONS

Nitrogen use efficiency (NUE) in spring wheat was strongly influenced by nitrogen fertilization level, year-specific environmental conditions, and genotype. Lower fertilization consistently resulted in higher NUE, while considerable genetic variability indicated opportunities for breeding improvements. The clear interaction between management and environment provides a robust basis for testing the capacity of vegetation indices to capture differences in NUE across diverse conditions.

Although the relationships between vegetation indices (VIs) and NUE were environmentally dependent, significant and robust correlations were identified. In general, proximal sensing platforms provided comparatively stronger prediction models for NUE. The Normalized Green-Red Difference Index (NGRDI) and Green Area Index (GA) consistently emerged as the most reliable predictors across three years, with the milk growth stage (GS75) proving to be the optimal timing for NUE estimation. Comparisons of NGRDI between proximal and UAV-based platforms confirmed the comparability of visible-spectrum canopy reflectance indices, though UAVs offer higher throughput in data acquisition.

Taken together, the results demonstrate that combining agronomic evaluation under contrasting N fertilization rates and environments with canopy reflectance traits enhances the capacity to phenotype NUE. This highlights the potential of low-cost proximal and UAV sensing platforms to complement traditional destructive methods and support both breeding and precision nitrogen management.

ACKNOWLEDGEMENTS. Research was done in EEA/Baltic Research Programme grant project ‘NOBALwheat–breeding toolbox for sustainable food system of the NOrdic BALtic region’, Nr. S-BMT-21-3 (LT08-2-LMT-K-01-032).

REFERENCES

Abreu, A.L., Ferraz, G.A.S., Morais, R., Bento, N.L., Conti, L., Bambi, G. & Ferraz, P.F.P. 2024. Use of geostatistical analyses for wheat production areas throung the variables NDVI, surface temperature and yield. *Agronomy Research* **22**(S1), 329–345. https://doi.org/10.15159/AR.24.021

Änäkkälä, M., Lehtilä, A., Mäkelä, P.S.A. & Lajunen, A. 2023. Application of UAV multispectral imaging for determining the characteristics of maize vegetation. *Agronomy Research* **21**(2), 644–653. https://doi.org/10.15159/AR.23.035

De Santis, M.A., Meloni, R., De Vita, P., Pecchioni, N., Reyneri, A., Flagella., Z., Blandino, M. 2025. Spectral phenotyping of agronomic and NUE traits in bread and durum wheat genotypes grown under two contrasting Mediterranean environments and different N fertilization strategies. *European Journal of Agronomy* **170** 127752. doi.org/10.1016/j.eja.2025.127752

Domínguez, J.A., Kumhálová, J. & Novák, P. 2017. Assessment of the relationship between spectral indices from satellite remote sensing and winter oilseed rape yield. *Agronomy Research* **15**(1), 055–068.

Feng, H., Tao, H., Li, Z., Yang, G. & Zhao, C. 2022. Comparison of UAV RGB Imagery and Hyperspectral Remote-Sensing Data for Monitoring Winter Wheat Growth. *Remote Sensing* **14**(15), 3811. doi.org/10.3390/rs14153811

Frels, K., Guttieri, M., Joyce, B., Leavitt, B. & Baenziger, P.S. 2018. Evaluating canopy spectral reflectance vegetation indices to estimate nitrogen use traits in hard winter wheat. *Field Crops Research* **217**, 82–92. doi.org/10.1016/j.fcr.2017.12.004

Fu, Y., Yang, G., Li, Z., Song, X., Li, Z., Xu, X., Wang, P. & Zhao, C. 2020. Winter wheat nitrogen status estimation using uav-based rgb imagery and gaussian processes regression. *Remote Sensing* **12**(22), 3778. doi:10.3390/rs12223778

Gano, B., Bhadra, S., Vilbig, J.M., Ahmed, N., Sagan, V. & Shakoor, N. 2024. Drone-based imaging sensors, techniques, and applications in plant phenotyping for crop breeding: A comprehensive review. *The Plant Phenome J.* **7(1**/e20100). doi.org: 10.1002/ppj2.20100

Ge, H., Xiang, H., Ma, F., Li, Z., Qiu, Z., Tan, Z. & Du, C. 2021. Estimating Plant Nitrogen Concentration of Rice through Fusing Vegetation Indices and Color Moments Derived from UAV-RGB Images. *Remote Sensing* **13**, 1620. doi.org/10.3390/rs13091620

Hamdane, Y., Segarra, J., Buchaillot, M.L., Rezzouk, F.Z., Gracia-Romero, A., Vatter, T., Benfredj, N., Hameed, R.A., Gutiérrez, N.A. & Torró, I. 2023. Using Ground and UAV Vegetation Indexes for the Selection of Fungal-Resistant Bread Wheat Varieties. *Drones* **7**, 454. doi.org/10.3390/drones7070454

Hawkesford, M. & Griffiths, S. 2019. Exploiting genetic variation in nitrogen use efficiency for cereal crop improvement. *Current Opinion in Plant Biology* **49**, 35–42. doi:10.1016/j.pbi.2019.05.003

Hunt, E.R., Cavigelli, M., Daughtry, C.S., McMurtrey, J.E. & Walthall, C.L. 2005. Evaluation of digital photography from model aircraft for remote sensing of crop biomass and nitrogen status. *Precis. Agric*. **6**, 359–378. doi:10.1007/s11119-005-2324-5

Jansone, Z., Rendenieks, Z., Lapaans, A., Tamm, I., Ingver, A., Gorash, A., Aleliunas, A., Brazauskas, G., Shafiee, S., Mróz, T., Lillemo, M., Kollist, H. & Bleidere, M. 2024. Phenotypic Variation and Relationships between Grain Yield, Protein Content and Unmanned Aerial Vehicle-Derived Normalized Difference Vegetation Index in Spring Wheat in Nordic–Baltic Environments. *Agronomy* **14**(1), 51. doi.org/10.3390/agronomy14010051

Jauregui-Besó, J., Gracia-Romero, A., Carrera, C.S., da Silva Lopes, M., Araus, J.L., Kefauver, S.C. 2025. Winter wheat plant density determination: Robust predictions across varied agronomic conditions using multiscale RGB imaging. *Smart Agricultural Technology* **11**, 100921. doi.org/10.1016/j.atech.2025.100921

Jelínek, Z., Starý, K., Kumhálová, J., Lukáš, J. & Mašek, J. 2020. Winter wheat, winter rape and poppy crop growth evaluation with the help of remote and proximal sensing measurements. *Agronomy Research* **18**(3), 2049–2059. https://doi.org/10.15159/AR.20.176

Kefauver, S. 2018. University of Barcelona, Barcelona, Spain. Available online: https://gitlab.com/sckefauver/MosaicTool/ (accessed on 25 September 2021)

Kefauver, S.C., Romero, A.G., Buchaillot, M.L, Diaz, O.V., Fernandez-Gallego, J.A, El-Haddad, G., Akl, A. & Araus, J.L. 2020. Open-Source Software for Crop Physiological Assessments Using High Resolution RGB Images. IGARSS 2020 - 2020 IEEE International Geoscience and Remote Sensing Symposium, 26 September 2020 - 02 October, Waikoloa, HI, USA 4359–4362. [Online]. Available: IEEXplore, https://ieeexplore.ieee.org/document/9324132 [Accessed February 15, 2025], doi:10.1109/IGARSS39084.2020.9324132

Kefauver, S.C., Vicente, R., Vergara-Díaz, O., Fernandez-Gallego, J.A., Kerfal, S., Lopez, A., Melichar, J.P.E., Serret Molins, M.D. & Araus, J.L. 2017. Comparative UAV and Field Phenotyping to Assess Yield and Nitrogen Use Efficiency in Hybrid and Conventional Barley. *Front. Plant Sci.* **8**, 1733. doi.org/10.3389/fpls.2017.01733

Li, R., Wang, D., Zhu, B., Liu, T., Sun, C. & Zhang, Z. 2022. Estimation of nitrogen content in wheat using indices derived from RGB and thermal infrared imaging. *Field Crops Research* **289**, 108735. doi.org/10.1016/j.fcr.2022.108735

Litke, L., Gaile, Z. & Ruža, A. 2018. Effect of nitrogen fertilization on winter wheat yield and yield quality. *Agronomy Research* **16**(2), 500–509. https://doi.org/10.15159/AR.18.064

Liu, J., Zhu, Y., Tao, X., Chen, X. & Li, X. 2022. Rapid prediction of winter wheat yield and nitrogen use efficiency using consumer-grade unmanned aerial vehicles multispectral imagery. *Front. Plant Sci*. **13**, 1032170. doi: 10.3389/fpls.2022.1032170

Malinas, A., Vidican, R., Rotar, I., Malinas, C., Moldovan, C.M. & Proorocu, M. 2022. Current Status and Future Prospective for Nitrogen Use Efficiency in Wheat (*Triticum aestivum* L.). *Plants* **11**(2), 217. doi: 10.3390/plants11020217

Moll, R.H., Kamprath, E.J. & Jackson, W.A. 1982. Analysis and interpretation of factors which contribute to efficiency of nitrogen utilization. *Agronomy Journal* **74**(3), 562–564. doi: 10.2134/agronj1982.00021962007400030037x

Pour, M.K., Fotouhi, R., Hucl, P. & Zhang, Q. 2021. Development of a Mobile Platform for Field-Based High-Throughput Wheat Phenotyping. *Remote Sens*. **13**(8), 1560. doi.org/10.3390/rs13081560

Prey, L. & Schmidhalter, U. 2019. Temporal and Spectral Optimization of Vegetation Indices for Estimating Grain Nitrogen Uptake and Late-Seasonal Nitrogen Traits in Wheat. *Sensors* **19**(21) 4640. doi.org/10.3390/s19214640

Prey, L., Hu, Y. & Schmidhalter, U. 2020. High-Throughput Field Phenotyping Traits of Grain Yield Formation and Nitrogen Use Efficiency: Optimizing the Selection of Vegetation Indices and Growth Stages. *Frontiers in Plant Science* **10**, 1672–1672. doi: 10.3389/fpls.2019.01672

Prey, L., Hanemann, A., Ramgraber, L., Seidl-Schulz, J. & Noack, P.O. 2022. UAV-Based Estimation of Grain Yield for Plant Breeding: Applied Strategies for Optimizing the Use of Sensors, Vegetation Indices, Growth Stages, and Machine Learning Algorithms. *Remote Sens.*, **14**, 6345. doi.org/10.3390/rs14246345

Quemada, M., Pancorbo, J.L., Alonso-Ayuso, M., Gabriel, J.L, Lopez-Herrera, J. & Perez-Martin, E. 2019. Vegetation indices from remote sensing imagery as proxies for yield and grain N in wheat. In: *Precision agriculture'19*, J. V. Stafford, Eds. Wageningen Academic Publichers, 323–330, doi.org/10.3920/978-90-8686-888-9_40

R Core Team. R: A Language and Environment for Statistical Computing; R Foundation for Statistical Computing: Vienna, Austria, 2021; Available online: https://www.R-project.org/ (accessed on 15 July 2024)

Rasmussen, J., Ntakos, G., Nielsen, J., Svensgaard, J., Poulsen, R.N. & Christensen, S. 2016. Are vegetation indices derived from consumer-grade cameras mounted on UAVs sufficiently reliable for assessing experimental plots. *Eur. J. Agron*. **74**, 75–92. doi.org/10.1016/j.eja.2015.11.026

Rossi, A., Tavarini, S., Tognoni, M., Angelini, L.G., Clemente, G. &Caturegli, L. 2025. Reliable NDVI estimation in wheat using low-Cost UAV-derived RGB vegetation indices. *Smart Agricultural Technology* **12** 101452. doi.org/10.1016/j.atech.2025.101452

Rui, Z., Zhang, Z., Zhang, M., Azizi, A., Igathinathane, C., Ced, H., Vougioukas, S., Li, H., Zhang, J., Jiao, X., Wang, M., Ampatzidis, Y., Oladele, O.I., Ghasemi-Varnamkhasti, M. & Radi, R. 2024. High-throughput proximal ground crop phenotyping systems – A comprehensive review. *Computers and Electronics in Agriculture* **224** 109108. doi.org/10.1016/j.compag.2024.109108

Shchuklina, O., Afanasiev, R., Gulevich, A., Baranova, A., Kvitko, A. & Kvitko, O. 2022. Using data of optic sensors and pigment content in leaves for efficient diagnostics of nitrogen nutrition. *Agronomy Research* **20**(4), 805–813. https://doi.org/10.15159/AR.22.048

Song, P., Wang, J., Guo, X., Yang, W., Zhao, C. 2021. High-throughput phenotyping: Breaking through the bottleneck in future crop breeding. *The Crop Journal* **9** (2021), 633–645. doi.org/10.1016/j.cj.2021.03.015

Tanaka, T.S.T., Wang, S., Jørgensen, J.R., Gentili, M., Vidal, A.Z., Mortensen, A.K., Acharya, B.S., Beck, B.D. & Gislum, R. 2024. Review of Crop Phenotyping in Field Plot Experiments Using UAV-Mounted Sensors and Algorithms. *Drones* **8**, 212. doi.org/10.3390/drones8060212

Vidican, R., Mălinas, A., Ranta, O., Moldovan, C., Marian, O., Ghet, A., Ghis, C.R., Popovici, F. & Cătunescu, G.M. 2023. Using Remote Sensing Vegetation Indices for the Discrimination and Monitoring of Agricultural Crops: A Critical Review. *Agronomy* **13**(12), 3040. doi.org/10.3390/agronomy13123040

Wang, Y., Wang, D., Zhang, G. & Wang, J. 2013. Estimating nitrogen status of rice using the image segmentation of G-R thresholding method. *Field Crops Res*. **149**, 33–39. doi.org/10.1016/j.fcr.2013.04.007

Xu, A., Chen, Y., Wei, X., Effah, Z., Li, L., Xie, J., Liu, C. & Anwar, S. 2024. Does Nitrogen Fertilization Improve Nitrogen-Use Efficiency in Spring Wheat? *Agronomy* **14**(9), 2049. doi.org/10.3390/agronomy14092049

Yang, M., Hassan, M.A., Xu, K., Zheng, C., Rasheed, A., Zhang, Y., Jin, X., Xia, X., Xiao, Y. & He, Z. 2020. Assessment of Water and Nitrogen Use Efficiencies Through UAV-Based Multispectral Phenotyping in Winter Wheat. *Front. Plant Sci*. **11**, 927. doi.org/10.3389/fpls.2020.00927

Zhang, L., Song, X., Niu, Y., Zhang, H., Wang, A., Zhu, Y., Zhu, X., Chen, L. & Zhu, Q. 2024. Estimating Winter Wheat Plant Nitrogen Content by Combining Spectral and Texture Features Based on a Low-Cost UAV RGB System throughout the Growing Season. *Agriculture* **14**, 456. doi.org/10.3390/agriculture14030456